Solvent Dependence of the Single Molecule Conductance of Oligoyne-Based Molecular Wires

David C. Milan,[1] Oday A. Al-Owaedi,[2,10] Marie-Christine Oerthel,[3] Santiago Marqués-González,[3] Richard J. Brooke,[4] Martin R. Bryce,[3] Pilar Cea,[5,6] Jaime Ferrer,[7] Simon J. Higgins,[1] Colin J. Lambert[*,2], Paul J. Low[3,8,*], David Zsolt Manrique,[2] Santiago Martin,[5,9] Richard J. Nichols,[1,*] Walther Schwarzacher,[4] Víctor M. García-Suárez.[7]

[1] Department of Chemistry, University of Liverpool, Liverpool, L69 7ZD, U.K.

[2] Department of Physics, Lancaster University, Lancaster LA1 4YB, U.K.

[3] Department of Chemistry, Durham University, Durham, DH1 3LE, U.K.

[4] HH Wills Physics Laboratory, University of Bristol, Bristol, BS8 1TL, U.K.

[5] Departamento de Química Física, Facultad de Ciencias, Universidad de Zaragoza, 50009 Zaragoza, Spain

[6] Instituto de Nanociencia de Aragón (INA) and Laboratorio de Microscopias Avanzadas (LMA), Edificio I+D+i. Campus Rio Ebro, Universidad de Zaragoza, C/Mariano Esquillor, s/n, 50018 Zaragoza, Spain.

[7] Nanomaterials and Nanotechnology Research Center and Physical Department, University of Oviedo & CSIC, 33007 Oviedo, Spain.

[8] School of Chemistry and Biochemistry, University of Western Australia, 6009, Australia.

[9] Instituto de Ciencia de Materiales de Aragón (ICMA), Universidad de Zaragoza-CSIC, 50009 Zaragoza, Spain.

[10]Department of Laser Physics, Women Faculty of Science, Babylon University, Iraq.

*Corresponding authors: c.lambert@lancaster.ac.uk, paul.low@uwa.edu.au, nichols@liv.ac.uk

ABSTRACT

The conductance, and the decay of conductance, as a function of molecular length within a homologous series of oligoynes, Me_3Si-$(C{\equiv}C)_n$-$SiMe_3$ (n = 2, 3, 4, 5) is shown to depend strongly on the solvent medium. Single molecule junction conductance measurements have been made with the *I*(s) method for each member of the series Me_3Si-$(C{\equiv}C)_n$-$SiMe_3$ (n = 2, 3, 4 and 5) in mesitylene (MES), 1,2,4-trichlorobenzene (TCB) and propylene carbonate (PC). In mesitylene, a lower conductance is obtained across the whole series with a higher length decay ($\beta \approx 1$ nm^{-1}). In contrast, measurements in 1,2,4 trichlorobenzene and propylene carbonate give higher conductance values with lower length decay ($\beta \approx 0.1$ nm^{-1}, $\beta \approx 0.5$ nm^{-1} respectively). This behavior is rationalized through theoretical and computational investigations, where β values are found to be higher when the contact Fermi energies are close to the middle of the HOMO-LUMO gap, but decrease as the Fermi energies approach resonance with either the occupied or unoccupied frontier orbitals. The different conductance and β values between MES, PC and TCB have been further explored using DFT-based models of the molecular junction, which include solvent molecules interacting with the oligoyne backbone. Good agreement between the experimental results and these 'solvated' junction models is achieved, giving new insights into how solvent can influence charge transport in oligoyne-based single molecule junctions.

KEYWORDS: STM, single molecule electronics, molecular conductance, scanning tunneling microscopy.

INTRODUCTION

Oligoynes hold particular interest in molecular electronics as the ultimate one-dimensional molecular wires formed from simple linear strings of *sp*-hybridized carbon atoms.[1-6] In

contrast to an infinite one-dimensional carbon string, oligoynes are terminated at either end by protons (H), organic, inorganic or organometallic moieties, and can be represented by the general formula R-(C≡C)$_n$-R. The terminating groups, R, can be chosen to aid the formation of metal-molecule-metal junctions, with examples including pyridyl, cyano, dihydrobenzo[*b*] thienyl and other anchoring groups.[3,4,7,8] Oligoynes feature extensive electron delocalization along the *sp*-hybridized carbon backbone, with appreciable bond length alternation evidenced in structural studies.[9] The presence of delocalized states makes oligoynes attractive targets for both theoretical and experimental studies of ultra-thin wires for molecular electronics. Single molecule wires of oligoynes have been experimentally investigated up to octa-1,3,5,7-tetraynes (n = 4),[3,4] while theoretical evaluations have been made for hypothetical infinitely long chains as well as finite chains.[1] However, it would be wrong to assume that oligoynes offer rigid-rod linear geometries; on the contrary they can be considerably curved and flexible offering a surprisingly low bending force.[9] Nevertheless, this structural flexibility does not detract from the impressive electronic properties of oligoynes, which offer considerable interest for their electronic, opto-electronic and electrical charge transport properties.[10]

Despite their apparent chemical simplicity it is a challenge to synthesize long carbon chains due to potential instability of R-(C≡C)$_x$-H intermediates and also instability of the longer oligoyne products for certain, particularly small, R groups. This issue was circumvented by Bohlmann who introduced bulky tertiary butyl (^{t}Bu) end groups in an n = 7 oligomer (^{t}Bu-(C≡C)$_7$-^{t}Bu), [11] and then also by Johnson and Walton, who extended the chain to ^{t}Bu-(C≡C)$_{12}$-^{t}Bu. [12] It has also been shown that in addition to a wide range of other bulky organic capping groups, cyano, aryl or organometallic terminal groups can stabilize oligoyne chains.[13] A recent approach to oligoyne stabilization has been “insulation” of the oligoyne by

threading through the cavity of a macrocycle, to give a rotaxane.[14-17] Metal centers have also been widely used as stabilizing end-caps to give complexes with the stoichiometry, $[\{L_mM\}\{\mu\text{-}(C\equiv C)_n\}\{ML_m\}]^{x+}$, which have provided interesting test-beds for examination of their electronic, physical and chemical properties as a function of metal oxidation state.[18] In particular, electronic and vibrational spectroscopies of complexes of this type, coupled with detailed computational investigations, have enabled electronic structures of the all-carbon chain bridged complexes to be assessed. [19] More direct assessment of the electrical properties of oligoynes can be achieved by wiring them into electrical junctions with metal contacts.[4,20]

Here we report conductance measurements of novel molecular wires $Me_3Si\text{-}(C\equiv C)_n\text{-}SiMe_3$ (n = 2, 3, 4, 5; Scheme 1), using STM-based techniques. In particular the influence of the solvent on conductance and β-values has been investigated. The molecular wires chosen here represent a strong choice for experimental investigations of solvent effects since they would be expected to be less effected by the small amounts of water present in even ostensibly well dried organic solvents. In this respect, it is mentioned that they have no functional groups in the backbone to coordinate the water (c.f. the gating by water of thiophene-based molecules[21]), and no thiol end groups to be hydrated and thereby adversely affect the conductance (c.f. ref. [22]). The experimental measurements of molecular conductance are complemented by density functional theory (DFT) computations of charge transport through the molecular bridge. Using DFT changes in the conductance and β values in response to the solvent medium are explained by shifts in the Fermi energy of the contact, which impacts on both the transmission coefficient of the systems and the β-value.

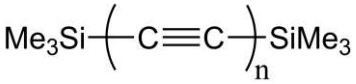

2 (n = 2) **4** (n = 4)
3 (n = 3) **5** (n = 5)

Scheme 1: The molecules studied in this work.

EXPERIMENTAL AND THEORETICAL METHODS

General details.

All reactions were carried out in oven-dried glassware under oxygen-free argon atmosphere. NEt_3 was purified by distillation from $CaSO_4$, other reaction solvents were purified and dried using Innovative Technology SPS-400 and, if necessary, degassed before use. The compounds $AuCl(PPh_3)$,[23] Me_3Si-$(C{\equiv}C)_3$-$SiMe_3$,[24] $HC{\equiv}CC{\equiv}CSiMe_3$,[25] $IC{\equiv}CC{\equiv}CSiMe_3$,[26] $Pd(PPh_3)_4$[27] were prepared by the literature methods. Other reagents were purchased commercially and used as received. NMR spectra were recorded in deuterated solvent solutions on Bruker Avance 400 MHz and Varian VNMRS 700 MHz spectrometers and referenced against residual protio-solvent resonances after nuclei ($CHCl_3$: ^{1}H 7.26 ppm, ^{13}C 77.00 ppm; $(CD_3)_2CO$: ^{1}H 2.05 ppm, ^{13}C 29.84 and 206.26 ppm) or H_3PO_4 (^{31}P). In the NMR assignment, the phenyl rings associated with the PPh_3 ligand are denoted Ph.

Mass spectra were measured on a Waters Xevo OtoFMs with an Atmospheric Solids Analysis Probe (ASAP). Electron ionization mass spectra were recorded on a Thermoquest Trace or Thermo-Finnigan DSQ. Infrared spectra were recorded on a Thermo 6700 spectrometer in CH_2Cl_2 solution in a cell fitted with CaF_2 windows. Elemental analyses were performed on a CE-400 Elemental Analyzer. Single-crystal X-ray data were collected at 120(2) K on a Bruker SMART CCD 6000 (fine-focus sealed tube, graphite-monochromator).

1,8-Bis(trimethylsilyl)-1,3,5,7-octatetrayne[28]

A Schlenk flask was charged with $IC{\equiv}CC{\equiv}CSiMe_3$ (0.10 g, 0.40 mmol), $HC{\equiv}CC{\equiv}CSiMe_3$ (90.0 μL, 0.07 g, 0.60 mmol), $Pd(PPh_3)_4$ (6.8 mg, 0.06 mmol) and CuI (1 mg, 0.06 mmol) in a

degassed solution of NEt_3 (10 mL). The yellow solution was stirred overnight at room temperature, under argon. The mixture was purified on a silica gel column eluted with hexane to give the product as a yellow oil, which crystallized in air on standing. Yield: 0.09 g, 92%. ^{1}H NMR (400 MHz, $CDCl_3$): δ 0.20 (s, 18H, $SiMe_3$) ppm. ^{13}C {^{1}H} NMR (700 MHz, $CDCl_3$): δ 88.0, 87.8, 62.2, 62.1 (*C*≡), -0.6 ($SiMe_3$) ppm. MS (ASAP$^+$; *m/z*): 484.2 [2 M]$^+$. Anal. Calcd. for $C_{14}H_{18}Si_2$: C, 69.35; H, 7.48; found C, 69.25; H, 7.56. IR (CH_2Cl_2): ν(C≡C-$SiMe_3$) 2044 (s); 2150, 2016 cm^{-1}. The NMR data are consistent with the previous literature.[28]

1,6-bis(triphenylphosphine gold(I))-1,3,5-hexatriyne, (PPh_3)Au-C≡CC≡CC≡C-Au(PPh_3)

A 250 mL two-necked round-bottomed flask was charged with 1,6-bis(trimethylsilyl)hexa-1,3,5-triyne (0.22 g, 1.0 mmol), AuCl(PPh_3) (0.94 g, 1.9 mmol) and NaOH (0.78 g, 20 mmol) dissolved in MeOH (150 mL). The reaction mixture was stirred at room temperature for 42 h. The bright yellow suspension was filtered and the solvent was removed under vacuum to give a pale yellow solid. Yield: 0.95 g, 96%. Crystals suitable for X-ray diffraction were obtained by slow evaporation of a $CDCl_3$ solution. ^{1}H NMR (400 MHz, $CDCl_3$): δ 7.52 - 7.41 (m, 30H, Ph) ppm. ^{31}P{^{1}H} NMR (400 MHz, $CDCl_3$): 41.2 ppm. ^{13}C {^{1}H} NMR (101 MHz, $CDCl_3$): δ 134.2 (d, J = 13.8 Hz, Ph), 131.6 (Ph), 129.7 (Ph), 129.1 (d, J = 11.4 Hz, Ph), the other quaternary ^{13}C are not seen. MS (MALDI-TOF; *m/z*): 990.0 [M]$^+$. HR-ESI$^+$-MS: *m/z* calcd for $C_{42}H_{30}P_2{}^{197}Au_2H$ 991.1257; found 991.1232. Calcd. for $C_{42}H_{30}Au_2P_2$: C, 50.93; H, 3.05; found C, 50.82; H, 2.97. IR (CH_2Cl_2): ν(C≡C-Au) 2112 (br); 2691 (s) cm^{-1}. Crystal data: $C_{42}H_{30}Au_2P_2$, M = 990.53, orthorhombic, space group Fddd, *a* = 14.2261(7), *b* = 33.5370(11), *c* = 34.6372(11) Å, *U* = 16525.4(10) Å^3, F(000) = 7520, Z = 16, D_C = 1.593 mg/mm^3, μ = 7.196 mm^{-1}; 58717 reflections were collected , yielding 5765 unique data (R_{merg} = 0.0764). Final *w*R_2(F^2) = 0.0475 for all data (205 refined parameters), conventional R_1 (F) = 0.0314 (for 4421 reflections with I ≥ 2σ), GOF = 1.081.

1,10-Bis(trimethylsilyl)-1,3,5,7,9-decapentayne[28]

To a solution of degassed THF (90 mL) was added PPh_3Au-C≡CC≡CC≡C-$AuPPh_3$ (0.90 g, 0.91 mmol), 1-iodo-2-(trimethylsilyl)acetylene (52 mg, 0.28 mL, 1.82 mmol), $Pd(PPh_3)_4$ (52 mg, 0.04 mmol) and CuI (17 mg, 0.09 mmol). The solution was stirred at room temperature for 20 h under argon, dried and then the reaction mixture purified on a silica gel column eluted with hexane. The first band was collected giving a yellow solution, which was dried to yield a brown oil. Yield: 92 mg, 38%. ^{1}H NMR (400 MHz, $CDCl_3$): δ 0.21 (s, 18H, Si*Me*$_3$) ppm. ^{13}C {^{1}H} NMR (101 MHz, $CDCl_3$): δ 88.6, 87.7, 62.6, 62.2, 61.2 (*C*≡), -0.6 (Si*Me*$_3$) ppm. MS (ASAP$^+$; m/z): 266.1 $[M]^+$. HR-(ASAP$^+$)-MS m/z: calcd for $C_{16}H_{18}{}^{28}Si_2$ 266.0947; found 266.0940. IR (CH_2Cl_2): ν(C≡C-$SiMe_3$) 2027 (s); 2102 (s). The NMR data were consistent with the literature.[28]

Single molecule conductance measurements

An Agilent STM running Picoscan 5.3.3 software was used for all single molecule conductance measurements which were performed at room temperature in mesitylene, propylene carbonate and trichlorobenzene solutions. Molecular ad-layers were formed on Au(111) textured substrates. These commercially available (Arrandee) substrates were produced from gold on glass samples with a chromium adhesive layer, which were flame annealed immediately prior to use. Flame annealing involved gently heating the gold slide until it developed a slight orange glow. It was then kept in this state for approximately 30 s, but care was taken to ensure that the sample did not overheat. Molecular adsorption was achieved by placing the gold slide in a 0.2 mL solution of 1×10^{-4} M of the target molecule in either mesitylene, propylene carbonate or trichlorobenzene. Gold STM tips were fabricated from 0.25 mm Au wire (99.99%) which was freshly electrochemically etched for each experiment at +7 V in a mixture of ethanol (50%) and conc. aqueous HCl (50%).

Electrical measurements were performed using an STM and the *I*(*s*) method [29-31] in the solvent of choice, which was degassed with argon. In brief, this method involves the repeated formation and cleavage of molecular bridges generally formed between gold contacts (an Au STM tip and an Au substrate). The *I*(*s*) method differs to the in-situ STM break junction method of Xu and Tao[32] in that metallic contact between the Au STM tip and substrate is avoided. In the *I*(*s*) technique the STM tip is moved toward the surface to a close distance determined by the STM set point conditions, but avoiding metallic contact between tip and surface, and then rapidly retracted.[29-31] In these measurements the *I*(*s*) process involves repeating this cycle many times, with a fraction of these approach/retraction cycles leading to the formation of molecular bridges. Such events are recognized during the retraction process as current steps characteristic of the cleavage of Au|molecule(s)|Au electrical junctions. At least 500 such junction forming scans, with plateaus longer than 1 Å, were recorded and used in the histogram analysis. *I*(*s*) traces are not included for scans where there are no characteristic steps to avoid the ambiguity of inclusion of traces where no molecular junction is formed. In this work we have performed *I*(*s*) scans from the position defined by the set-point values of tunneling current (I_0) and tunneling voltage (U_t) to a distance of +4 nm with a STM tip retraction rate of 20 nm s^{-1}. Set point values of I_0 = 30 nA and a bias voltage of 0.6 V were employed to ensure that the STM tip initially approached the surface to distances much shorter than the molecular length to promote molecular junction formation. The voltage to length conversion factor of the STM was calibrated using images of Au(111) monatomic steps (0.235 nm height).

Theoretical Details

Computational Methods

The DFT-Landauer approach used in the modeling assumes that on the timescale taken by an electron to traverse the molecule, inelastic scattering is negligible. This is known to be an

accurate assumption for molecules up to several nm in length.[33] Geometrical optimizations were carried out using the DFT code SIESTA, with a generalized gradient approximation[34,35] (PBE functional), double-zeta polarized basis set, 0.01 eV/A force tolerance and 250 Ry mesh cutoff. All molecules in this study were initially geometrically relaxed in isolation to yield the geometries presented in the results section.

For each structure, the transmission coefficient *T(E)* describing the propagation of electrons of energy *E* from the left to the right electrode was calculated by first obtaining the corresponding Hamiltonian and overlap matrices using SIESTA, and then using the GOLLUM code[36] to compute *T(E)* via the relation

$T(E) = \mathrm{Tr}\{\Gamma_R(E)G^R(E)\Gamma_L(E)G^{R\dagger}(E)\}$.

In this expression, $\Gamma_{L,R}(E) = i\left(\sum_{L,R}(E) - \sum_{L,R}{}^{\dagger}(E)\right)$ describes the level broadening due to the coupling between left (L) and right (R) electrodes and the central scattering region, $\sum_{L,R}(E)$ are the retarded self-energies associated with this coupling and $G^R = (ES - H - \sum_L - \sum_R)^{-1}$ is the retarded Green's function, where *H* is the Hamiltonian and *S* is the overlap matrix (both of them obtained from SIESTA). Finally the room temperature electrical conductance *G* was computed from the formula $G = G_0 \int_{-\infty}^{\infty} dE\, T(E)(-\frac{df(E)}{dE})$ where $f(\mathrm{E}) = [e^{\beta(E-E_F)} + 1]^{-1}$ is the Fermi function, $\beta = 1/k_BT$, E_F is the Fermi energy and $G_0 = \left(\frac{2e^2}{h}\right)$ is the quantum of conductance. Since the quantity $(-\frac{df(E)}{dE})$ is a probability distribution peaked at $E=E_F$, with a width of the order k_BT, the above expression shows that G/G_0 is obtained by averaging $T(E)$ over an energy range of order k_BT in the vicinity of $E=E_F$. It is well-known that the Fermi energy E_F^{DFT} predicted by DFT is not usually reliable and therefore we show later plots of G/G_0 as a function of $E_F - E_F^{DFT}$. To determine E_F, we compared the predicted values of all molecules with the experimental values and chose a single common value of E_F which gave the closest overall agreement. This yielded a value of $E_F - E_F^{DFT} = -0.725$ eV, which is used

in all theoretical results. In addition, the Fermi energy may depend on the environment (solvent). To determine E_F we compared the calculated β values to experimental data and chose those Fermi energies where we found agreement.

RESULTS AND DISCUSSION

The family of trimethylsilyl end-capped oligoynes Me_3Si-$(C{\equiv}C)_n$-$SiMe_3$ (n = 2 – 5) were chosen as the platform upon which to base the investigations of molecular conductance and solvent-effects in wire-like oligoyne derivatives. These compounds are readily available, syntheses of oligoynes Me_3Si-$(C{\equiv}C)_n$-$SiMe_3$ (n = 2,[37,38] 3 [24]) being well known, whilst the diyne (n = 2) is also available commercially. For the octatetrayne, existing synthetic routes range from a homo coupling of 4-trimethylsilylbuta-1,3-diyne under Hay conditions[39] to a Stille-style cross-coupling between 1,4-diiodobuta-1,3-diyne and 1-trimethylsilyl-2-trimethylstannyl acetylene.[28] Here, oligoyne Me_3Si-$(C{\equiv}C)_4$-$SiMe_3$ was prepared in very good yield (92%) from a Cadiot-Chodiewicz inspired cross-coupling reaction[26] of 1-iodo-4-trimethylsilylbuta-1,3-diyne[25] and 1-trimethylsilylbuta-1,3-diyne.[40] The longest oligoyne Me_3Si-$(C{\equiv}C)_5$-$SiMe_3$ was prepared from 1,6-bis-triphenylphosphinegold-hexa-1,3,5-triyne through a double cross-coupling[41-44] with 1-iodo-2-(trimethylsilyl)acetylene.

The trimethylsilyl moiety –$SiMe_3$ (TMS) was chosen as the oligoyne end-cap and contacting group to the gold surfaces (substrate and STM tip) for a number of reasons. The synthesis of oligoynes with TMS terminal groups is relatively uncomplicated and leads to stable analogues, which is not necessarily expected to be the case for some other contacting groups such as thiols. In addition, molecular wires with trimethylsilylethynyl (-$C{\equiv}CSiMe_3$ or TMSE) groups have shown a single low conductance peak in conductance histograms, which has been attributed to its steric bulk, which limits the range of conductive junction

configurations.[45,46] The resulting narrow and sharp conductance peaks allow us to measure the shift of the conductance values with greater certainty. Also in the case of other more polar surface contacting groups, such as thiols, solvation of the contacting group has been proposed to have a major effect on conductance. [22] Furthermore, it is expected that the relatively large footprint of the TMS linker will inhibit stacking and close approach of neighboring molecules. This is an important consideration as for certain classes of π-conjugated molecules, for instance oligo(phenylene)ethynylene (OPE) derivatives, it has been shown that proximal molecular bridges can π-stack in molecular electrical junctions and can, on occasions, give rise to additional complications in the conductance signatures of such compounds.[20,47]

The single molecule conductance of the oligoynes **2** - **5** was explored in each of three organic solvents of differing polarity, namely mesitylene (MES), trichlorobenzene (TCB) and propylene carbonate (PC). Mesitylene is a non-polar solvent with zero dipole moment and it is commonly used in STM based single molecule electrical measurements because of its high boiling point and relatively low vapor pressure.[48-50] TCB is also frequently used in STM based single molecule electrical measurements and like mesitylene it is a high boiling point and low vapor pressure organic solvent. However, it is a slightly polar solvent with a dipole moment of 1.35 D.[51] By contrast, propylene carbonate (PC) is a strongly dipolar solvent with a dipole moment of 4.9 D.

Figure 1 shows conductance histograms for **2**-**5** recorded in propylene carbonate which had been degassed with argon. These measurements required a preliminary study to check the effect of the propylene carbonate on the gold surface and, due to the polarity of this solvent, check the capacitive and faradaic background currents[16] (see Supplementary Figures S4-S8).

As can be seen from Figure 1 the conductance values decrease with the molecular length and the break-off distance histogram distributions shift to longer distance along the series. The diyne **2** (n = 2) shows a mean break-off distance of 1.3 nm and this increases to 2.0 nm for the pentayne (n = 5). Using the Si…Si distances computed from molecular modelling and a silicon to gold contact distance of 0.31 nm, also estimated from molecular modelling, gives a theoretical Au-to-Au junction separation of 1.4 nm for **2** and 2.1 nm for **5**. Figure 2 shows data recorded in a similar manner in TCB, while Figure 3 shows data recorded in mesitylene.

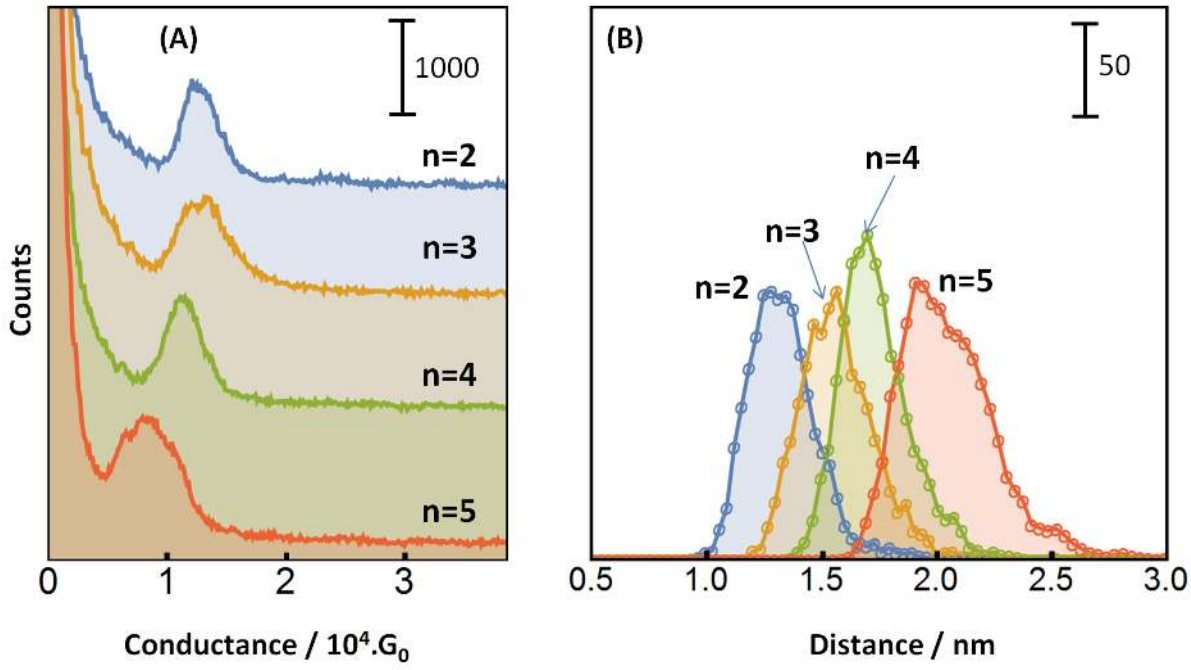

Figure 1: *I*(*s*) conductance (A) and break-off distance (B) histograms recorded for the series of oligoynes **2**, **3**, **4**, **5** in PC. Conductance histograms have been offset vertically for clarity.

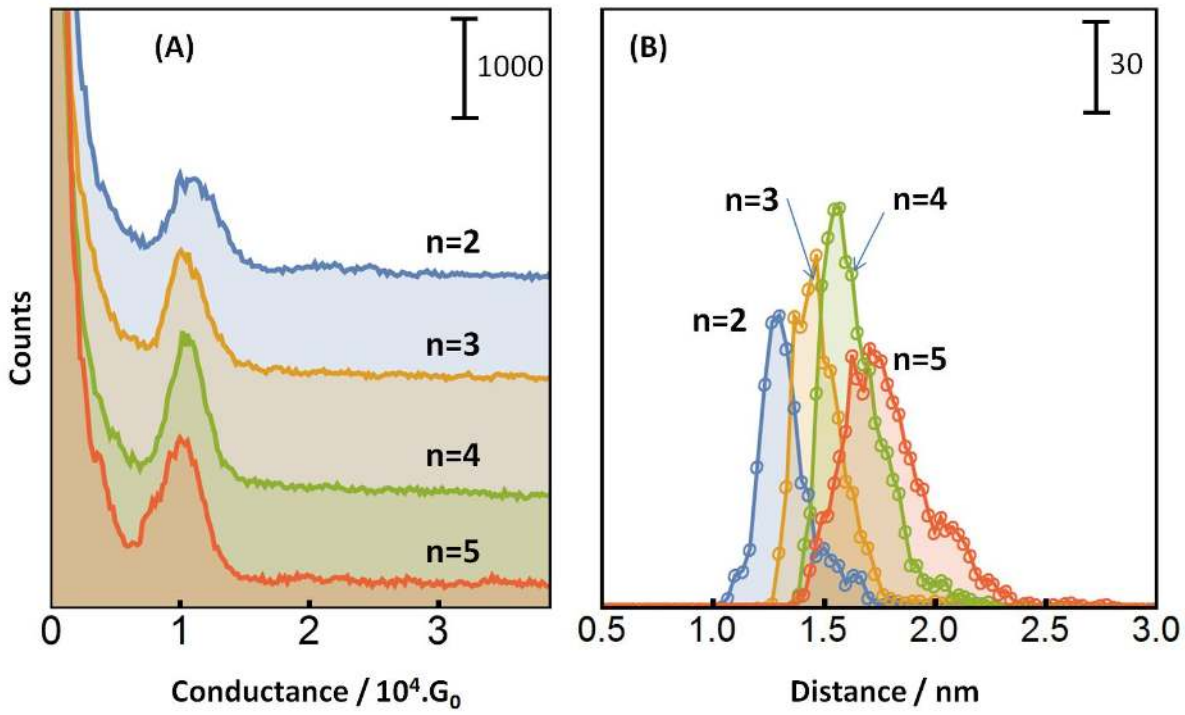

Figure 2: *I*(*s*) conductance (A) and break-off distance (B) recorded for the series of oligoynes **2**, **3**, **4**, **5** in TCB. Conductance histograms have been offset vertically for clarity.

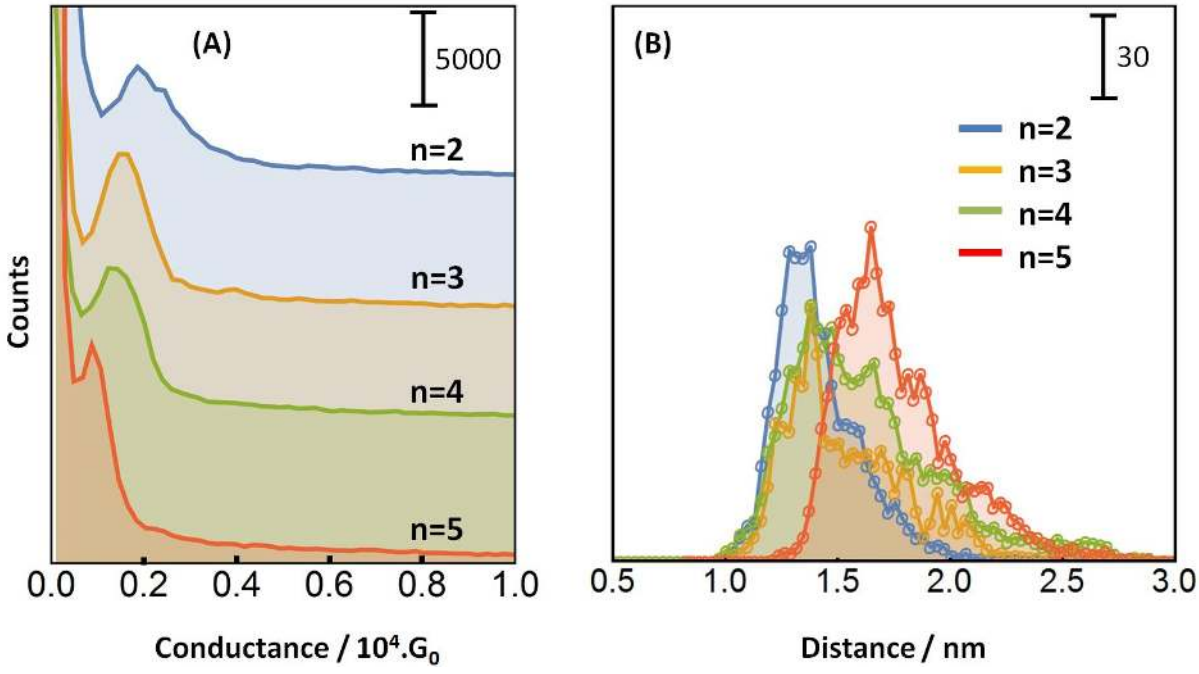

Figure 3: *I*(*s*) conductance (A) and break-off distance (B) recorded in mesitylene for **2**, **3**, **4**, **5**. Conductance histograms have been offset vertically for clarity.

The single molecule conductance data are summarized in Table 1 and Table S1 of the supporting information. A plot of ln(conductance) versus junction length is given in Figure 4. The conductance values are larger in TCB and PC than those obtained in mesitylene solutions. From this, it is apparent that the same molecule can give conductance values that vary significantly with the solvent medium. Not only does the conductance change, but different length decays are also obtained across the series of oligoynes as quantified by the β values (Figure 4). The β value recorded in mesitylene (0.94 nm^{-1}) is substantially higher than that in TCB (0.13 nm^{-1}) and PC (0.54 nm^{-1}); the corresponding experimentally determined β values per incremental –(C≡C)- unit are 0.26 (MES), 0.035 (TCB) and 0.145 (PC).

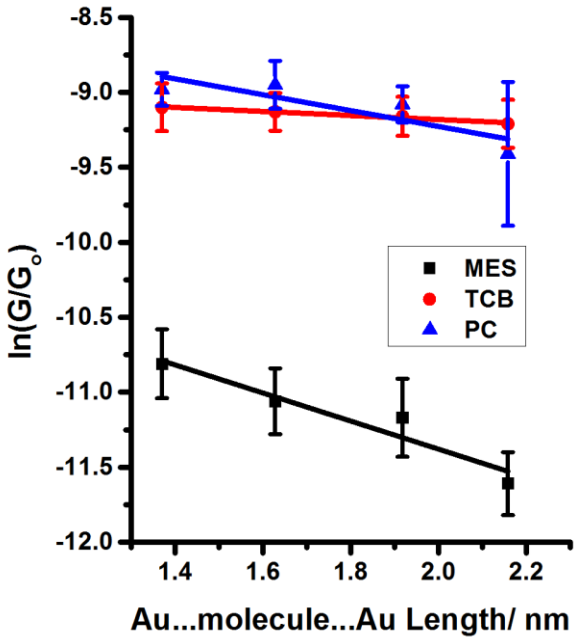

Figure 4: Plots of ln(conductance) versus junction length for the series **2**, **3**, **4**, **5**. Data recorded in mesitylene (MES), trichlorobenzene (TCB) and propylene carbonate (PC) as labelled. The linear fitting of each plot gives the β value of each solvent series.

Quantum Chemical Modelling

To gain a deeper insight into the role of the solvent medium and molecular length on molecular conductance, we turned to computational modeling. Before computing transport properties, all molecules were initially geometrically relaxed in isolation to yield the geometries shown in Figure 5. This figure shows that the HOMOs and LUMOs are extended across the backbone for each molecule, with HOMOs showing large contributions from the carbon-carbon triple bonds, while the LUMOs have greater contributions from the carbon-carbon single bonds, as expected from previous studies of oligoynes.[3,52-54]

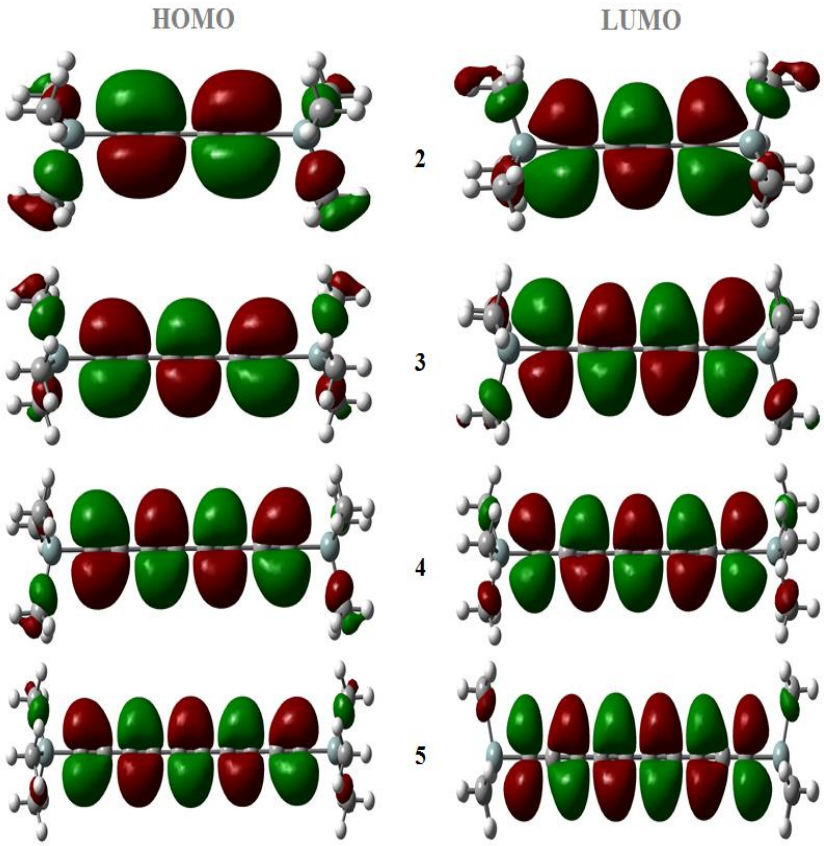

Figure 5: The iso-surfaces of the HOMOs and LUMOs for **2**-**5**.

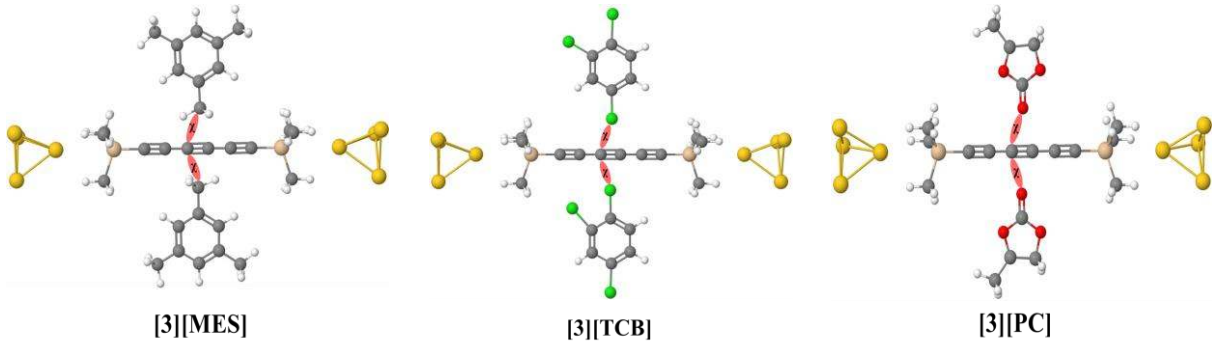

Figure 6: Definition of the distance (χ) used to describe the various geometries representing solvent-oligoyne interaction with **3** by way of an example. χ is the distance between carbon (grey), chlorine (green) or oxygen (red) atoms of the solvent molecules (MES, TCB or PC) and the nearest adjacent carbon atom of the backbone. For clarity only two of the six solvent molecules employed to represent the first solvation shell are shown in these schematic representations.

To explore how the solvent medium (MES, TCB or PC) affects the conductance of these molecules, six molecules of each solvent were initially placed at a nearest distance χ from the oligoyne backbone within the model junction (Figure 6). In each simulation the molecule plus solvent molecules together with a few layers of gold at each pyramidal electrode were allowed to relax. These simulations were carried out with seven different initial distances χ for each solvent as shown in Figure 7, resulting in seven different relaxed geometries. The relaxed structures are shown in Figure 8 for the three different solvents.

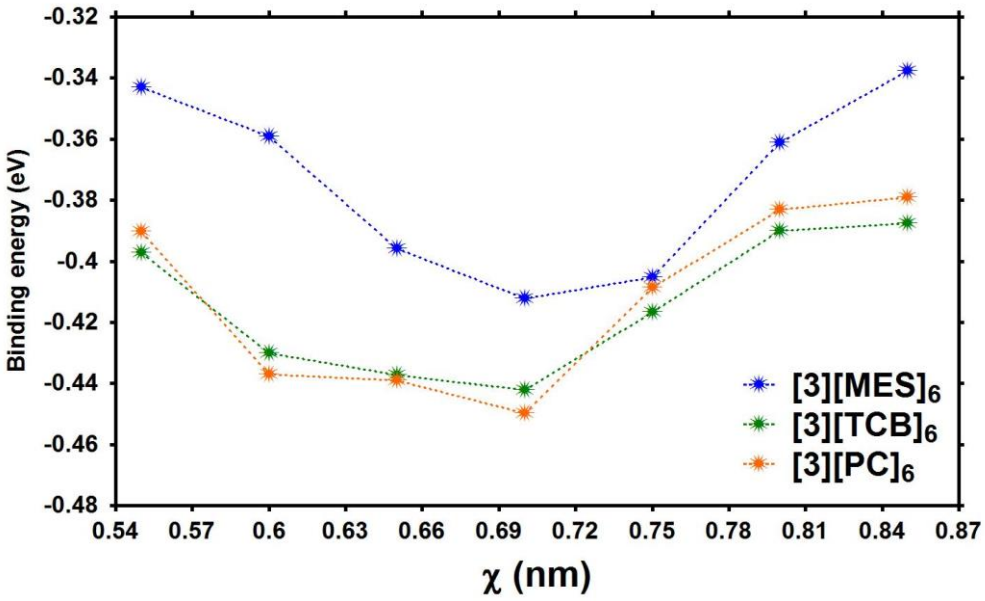

Figure 7: The binding energy between the gold contact and the TMS terminal group in **3** versus the distance between the solvent molecules and the backbone (χ).

Before calculating the transport properties of these structures, the binding energies were computed for the contact formed between the gold cluster and the TMS terminal groups for each of the different optimized distances, χ. Two points are noteworthy from the binding energy plots of Figure 7. First, for the junctions modeled in Figure 7 with compound **3** by way of an example, the optimized distance at which the contact binding energy reaches its maximum value is χ = 0.7 nm. Consequently, in what follows, the transport properties are calculated for the structures with the optimized distance χ = 0.7 nm. Secondly, the structures with TCB and PC solvation exhibit slightly stronger Au-TMS contact binding than for mesitylene solvation (-0.41 eV for the structures with MES, and -0.44 eV for the structures

with TCB and PC). However the differences in binding energies are small, and less than or of order of k_BT at room temperature.

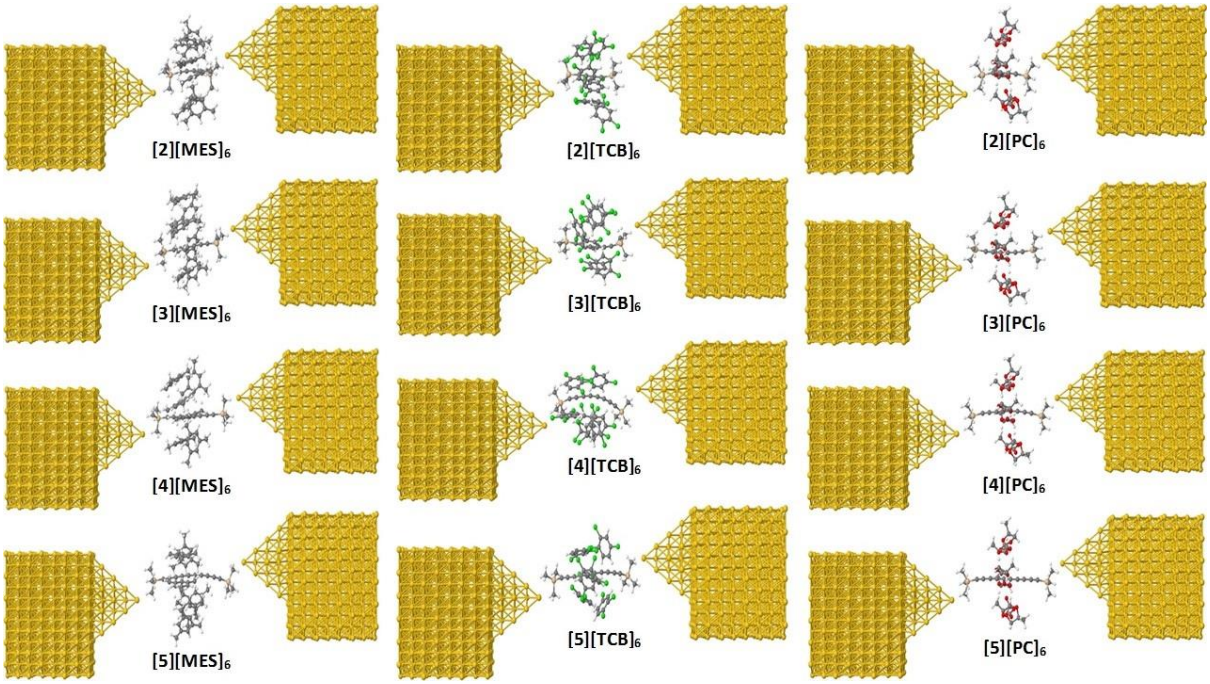

Figure 8: The relaxed structures of junctions incorporating **2-5** in each of three different solvents (MES, TCB and PC).

To investigate the electronic properties of these molecules in three different environments, we used the SIESTA code, which employs norm-conserving pseudopotentials and linear combination of atomic orbitals (LCAO) to span the valence states. All systems were initially placed between two pyramidal gold electrodes, and then the oligoyne molecule plus solvent molecules and a few layers of gold were allowed to relax to yield the structures. Then to calculate the transmission coefficient $T(E)$ using the GOLLUM code, the resulting configurations were connected to bulk gold electrodes grown along the (111) direction as shown in Figure 8 and described in detail elsewhere [36].

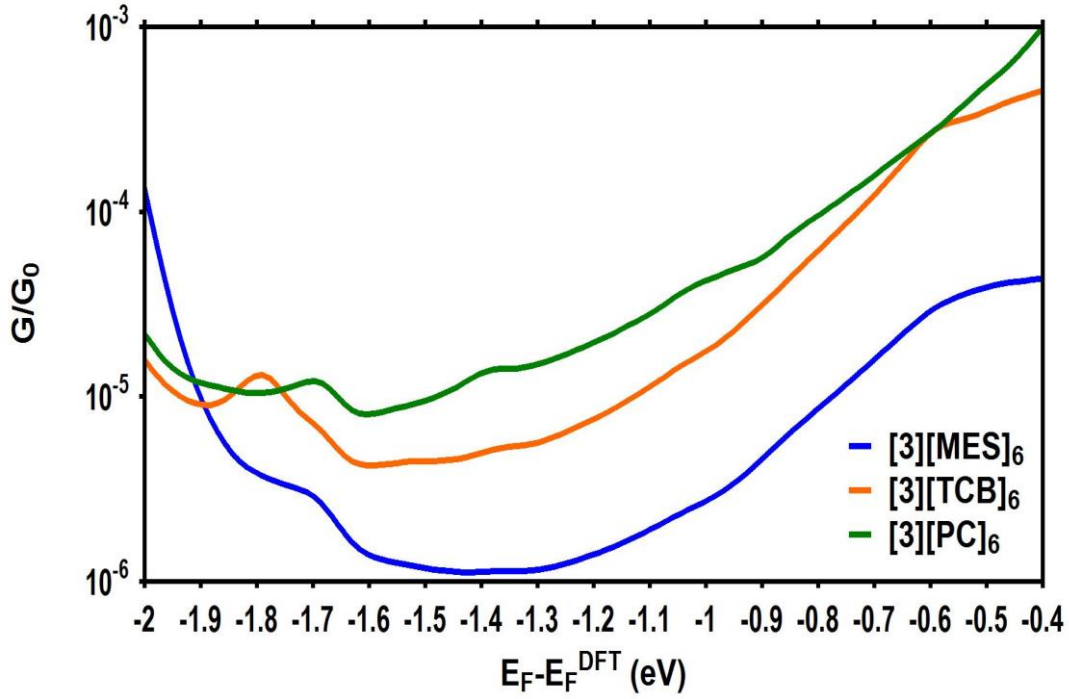

Figure 9: The room-temperature conductances as a function of the Fermi energy for **3** in mesitylene (MES), trichlorobenzene (TCB) and propylene carbonate (PC).

The theoretical and experimental data are summarized in Figures 9 (illustrated for **3** by way of an example), 10, 11 and Table 1. Figure 9 shows the calculated room temperature conductances (in $G/G(0)$), plotted for energies in the HOMO-LUMO gap region, as a function of the Fermi energy (E_F) for **3**, relative to the DFT-predicted Fermi energy (E_F^{DFT}) (see supplementary information Figure S8 for all conductance curves). Figure 9 is plotted for energies in the HOMO-LUMO gap region. Since DFT does not usually predict the correct value of the Fermi energy, we treat E_F as a free parameter which we determine by comparing the calculated decay constant with experiment.[55]

Figure 10 shows the Fermi energy dependence of the decay constant (β) for the molecular series **2**, **3**, **4** and **5** in MES, TCB and PC solutions, respectively. The best agreement with experimental data as shown in Figure 11 is obtained at E_F = -0.72 eV, which is shifted towards the center of the HOMO-LUMO gap, compared with the DFT-predicted value. With

this choice of E_F both computational (Figure 9) and experimental (Figure 4) data sets show that the order of the conductance at the chosen Fermi energy is PC ≈ TCB > MES. At E_F = -0.72 eV the computational β values (Figure 10) follow the trend $\beta_{MES} > \beta_{TCB} > \beta_{PC}$, meaning that the experimentally observed β value recorded in TCB is not so well reproduced by theory. However, it can be seen from Figure 10 that the β versus Fermi energy curve around the chosen E_F value has a high slope. This sensitivity to the precise Fermi energy value may explain this disparity.

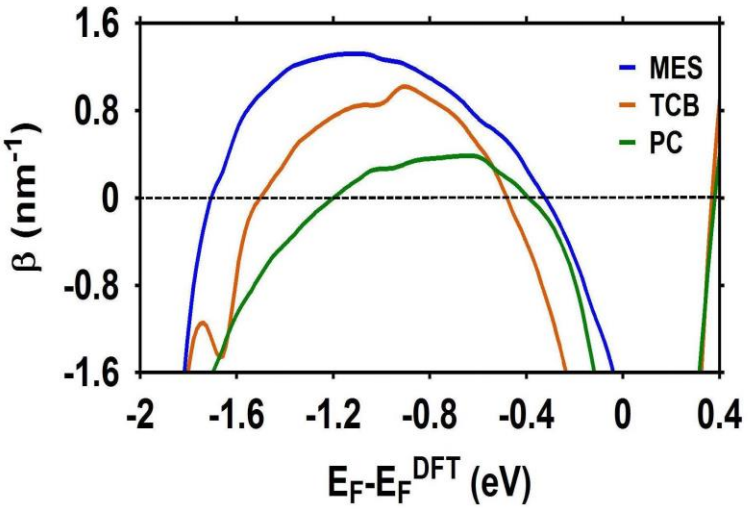

Figure 10: The decay constant β (nm^{-1}) for the molecular series **2**, **3**, **4** and **5** as a function of the Fermi energy in three different solvents (MES, TCB and PC).

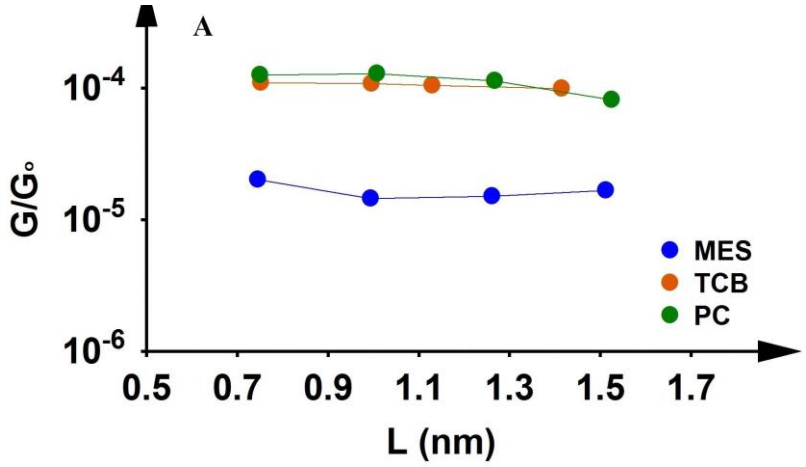

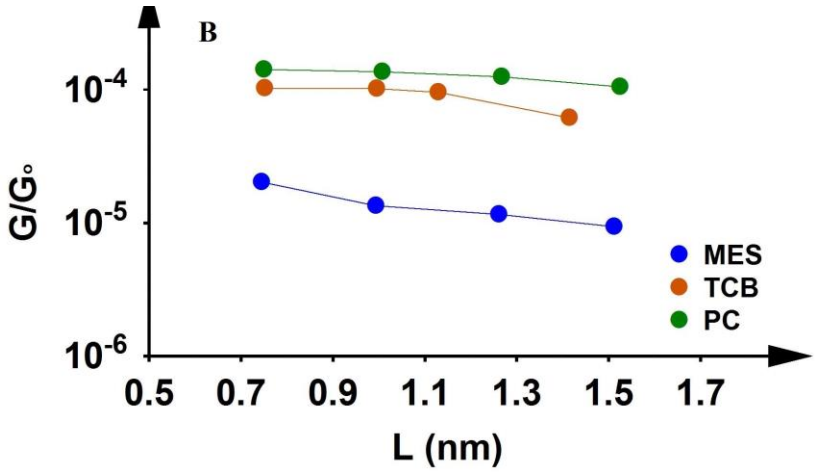

Figure 11: The conductance versus length for all molecules in three different solvents (MES, TCB and PC) as shown in Table 1. Panel A shows the experimental conductance (G/G_0) versus versus L (nm), where L is the distance between Si…..Si atoms; Panel B shows the calculated conductance G/G_0 versus L.

Figure 11 and Table 1 summarize and compare the experimental and theoretical conductance values versus the number of carbon-carbon triple bonds (n). We note here that for both experimental and computational data sets the conductance of the structures with PC and TCB is higher than that with MES.

n	MES		TCB		PC	
	Th. G/G_0	**Ex. G/G_0**	**Th. G/G_0**	**Ex. G/G_0**	**Th. G/G_0**	**Ex. G/G_0**
2	2.03×10^{-5}	2.02×10^{-5}	10.3×10^{-5}	11×10^{-5}	14.2×10^{-5}	12.6×10^{-5}
3	1.35×10^{-5}	1.57×10^{-5}	10.2×10^{-5}	10.8×10^{-5}	13.7×10^{-5}	12.9×10^{-5}
4	1.16×10^{-5}	1.42×10^{-5}	9.60×10^{-5}	10.5×10^{-5}	12.6×10^{-5}	11.3×10^{-5}
5	0.94×10^{-5}	0.90×10^{-5}	6.16×10^{-5}	9.95×10^{-5}	10.6×10^{-5}	8.14×10^{-5}
β (nm^{-1})	1.003	0.94	0.775	0.13	0.378	0.54
β(-C≡C-)	0.257	0.258	0.17	0.035	0.1	0.145

Table 1 The theoretical and experimental conductances and decay constant, in nm^{-1} (β (nm^{-1})) and per incremental –(C≡C)- unit, β(-C≡C-) in three different solvents (MES, TCB and PC).

Although oligoynes represent one of the most archetypical molecular wires the effects of solvents on their single molecule conductance has not been considered before. The calculations described above show that the solvent surrounding the oligoyne molecule bridge has a strong impact on the computed electron transmission curves for the junctions. As a result different conductance and length dependence values are obtained across the homologous series. This is not the result of covalent interactions between the solvent and the bridge, but rather occurs from longer range electrostatic interactions. This could be described as a "solvent induced gating of the molecular junction electrical properties".

Solvent effects have only been examined in detail in the literature for a relatively small number of single molecular junctions, which is perhaps surprising given that most measurements of this kind are performed in a liquid or ambient environment. Li et al. found the conductance values of octanedithiol to be independent of solvent (toluene, dodecane and water).[56] This is perhaps not unexpected given the very large HOMO-LUMO gap for this far-off-resonance tunneling system. On the other hand, Leary et al. have demonstrated large solvent dependence for the conductance of oligothiophene-containing molecular wires.[21] This was attributed to water molecules directly interacting with the thiophene molecular rings and thereby shifting transport resonances with the effect of greatly increasing conductance. Water dependence has also been seen in perylene tetracarboxylic diimides (PCTDI)- containing molecular bridges, with the measured conductance being temperature dependent in aqueous solvent, but temperature independent in toluene.[57] In a theoretical study of this system the water and temperature dependence was modelled through thermal effects on the hydrogen

bonding network interacting primarily with the carbonyl moieties on PCTDI.[58] Other models have considered the effect of the solvent on the gold contact work function. In such a study Fatemi et al. experimentally determined that solvents could increase the conductance of 1,4-benzenediamine (BDA)-gold molecular junctions by up to 50 %.[59] This was attributed to shifts in the gold contact Fermi energies resulting from solvent binding, leading to better alignment to the HOMO of BDA and hence higher conductance. These studies collectively show the complexity of solvent effects in molecular junctions, which have, depending on the system, been modelled through electrostatic interactions between the solvent and molecular bridges, chemical bonding between the solvent and molecular bridge, or through solvent binding to gold contact atoms. Our present study demonstrates that longer range solvent-molecular bridge interactions alone can describe the experimentally observed solvent effects on oligoyne junction conductance. Our study also rationalizes the previously unexpected differences observed between different studies of oligoyne molecular conductance,[3,4] which can be now attributed to solvent effects.

CONCLUSION

In conclusion, we have demonstrated that changing the solvent can lead to changes in both the conductance and the attenuation factor of oligoyne molecular bridges. DFT computations show that both the molecular junction conductance and the attenuation factors depend in a very sensitive manner on the position of the contact Fermi energies within in the HOMO-LUMO gap. These results show that the solvent environment is an important variable to consider in interpreting conductance measurements, and that the environment can give rise to dramatic changes in both conductance and attenuation factors.

Acknowledgments

D.C.M., S.J.H., R.J.N., P.J.L. and S.M-G. thank EPSRC for funding (EPSRC grants EP/K007785/1, EP/H035184/1 and EP/K007548/1). P.J.L. holds an ARC Future Fellowship

(FT120100073) and gratefully acknowledges funding for this work from the ARC (DP140100855). C. J. L. and O. A. A. acknowledge financial support from the Ministry of Higher Education and Scientific Research of Iraq. V.M.G.-S. thanks the Spanish Ministerio de Economía y Competitividad for a Ramón y Cajal fellowship (RYC-2010-06053). J.F. and V.M.G.-S. acknowledge financial support from the Spanish MICINN grant FIS2012-34858 and the Marie Curie Network MOLESCO. They also acknowledge the supercomputing facility CESGA where part of the calculations was carried out. P.C. and S.M. are grateful for financial assistance from Ministerio de Economía y Competitividad from Spain in the framework of the project CTQ2012-33198 as well as the award of the CTQ2013-50187-EXP grant. P.C and S.M. thank the DGA and Fondos FEDER for funding for the Platon research group. S.M. thanks the Ministerio de Educación of Spain for financial support in the framework of the Campus de Excelencia Internacional, CEI Iberus. M.R.B.and C. J. L. acknowledge funding from the EU through the FP7 ITN MOLESCO (project number 212942). We thank Dr Dmitry S. Yufit (Durham University) for determining the molecular structure of the 1,6-bis(triphenylphosphine gold(I))-1,3,5-hexatriyne complex.

Supporting Information Available: Summary of conductance and β values, analysis of the suitability of PC as a solvent for the junction conductance measurements, water content and conductivity of the solvents, x-ray crystallography of compounds, additional theoretical data. This material is available free of charge via the Internet at http://pubs.acs.org.

References

(1) Crljen, Z.; Baranovic, G. Unusual Conductance of Polyyne-Based Molecular Wires. *Phys. Rev. Lett.* **2007**, *98*, 116801.

(2) Garcia-Suarez, V. M.; Lambert, C. J. Non-Trivial Length Dependence of the Conductance and Negative Differential Resistance in Atomic Molecular Wires. *Nanotechnology* **2008**, *19*, 455203.

(3) Wang, C.; Batsanov, A. S.; Bryce, M. R.; Martin, S.; Nichols, R. J.; Higgins, S. J.; Garcia-Suarez, V. M.; Lambert, C. J. Oligoyne Single Molecule Wires. *J. Am. Chem. Soc.* **2009**, *131*, 15647-15654.

(4) Moreno-Garcia, P.; Gulcur, M.; Manrique, D. Z.; Pope, T.; Hong, W.; Kaliginedi, V.; Huang, C.; Batsanov, A. S.; Bryce, M. R.; Lambert, C.; Wandlowski, T.

Single-Molecule Conductance of Functionalized Oligoynes: Length Dependence and Junction Evolution. *J. Am. Chem. Soc.* **2013**, *135*, 12228-12240.

(5) Gibtner, T.; Hampel, F.; Gisselbrecht, J. P.; Hirsch, A. End-Cap Stabilized Oligoynes: Model Compounds for the Linear sp Carbon Allotrope Carbyne. *Chemistry-A European Journal* **2002**, *8*, 408-432.

(6) Slepkov, A. D.; Hegmann, F. A.; Eisler, S.; Elliott, E.; Tykwinski, R. R. The Surprising Nonlinear Optical Properties of Conjugated Polyyne Oligomers. *J. Chem. Phys.* **2004**, *120*, 6807-6810.

(7) Jia, C.; Guo, X. Molecule-Electrode Interfaces in Molecular Electronic Devices. *Chem. Soc. Rev.* **2013**, *42*, 5642-5660.

(8) Gulcur, M.; Moreno-Garcia, P.; Zhao, X.; Baghernejad, M.; Batsanov, A. S.; Hong, W.; Bryce, M. R.; Wandlowski, T. The Synthesis of Functionalised Diaryltetraynes and Their Transport Properties in Single-Molecule Junctions. *Chemistry-A European Journal* **2014**, *20*, 4653-4660.

(9) Szafert, S.; Gladysz, J. A. Carbon in One Dimension: Structural Analysis of the Higher Conjugated Polyynes. *Chem. Rev.* **2003**, *103*, 4175-4205.

(10) Palsson, L.-O.; Wang, C.; Batsanov, A. S.; King, S. M.; Beeby, A.; Monkman, A. P.; Bryce, M. R. Efficient Intramolecular Charge Transfer in Oligoyne-Linked Donor-Pi-Acceptor Molecules. *Chemistry-A European Journal* **2010**, *16*, 1470-1479.

(11) Bohlmann, F. Polyacetylene .4. Darstellung von Di-Tert-Butyl-Polyacetylenen. *Chem. Ber. Recl.* **1953**, *86*, 657-667.

(12) Johnson, T. R.; Walton, D. R. M. Silylation as a Protective Method in Acetylene Chemistry - Polyyne Chain Extensions Using Reagents, $Et_3Si(C{=}C)MH$ (M=1,2,4) in Mixed Oxidative Couplings. *Tetrahedron* **1972**, *28*, 5221-5236.

(13) Jevric, M.; Nielsen, M. B. Synthetic Strategies for Oligoynes. *Asian Journal Of Organic Chemistry* **2015**, *4*, 286-295.

(14) Sugiyama, J.; Tomita, I. Novel Approach to Stabilize Unstable Molecular Wires by Simultaneous Rotaxane Formation - Synthesis of Inclusion Complexes of Oligocarbynes with Cyclic Host Molecules. *Eur. J. Org. Chem.* **2007**, 4651-4653.

(15) Schrettl, S.; Contal, E.; Hoheisel, T. N.; Fritzsche, M.; Balog, S.; Szilluweit, R.; Frauenrath, H. Facile Synthesis of Oligoyne Amphiphiles and their Rotaxanes. *Chemical Science* **2015**, *6*, 564-574.

(16) Movsisyan, L. D.; Kondratuk, D. V.; Franz, M.; Thompson, A. L.; Tykwinski, R. R.; Anderson, H. L. Synthesis of Polyyne Rotaxanes. *Org. Lett.* **2012**, *14*, 3424-3426.

(17) Weisbach, N.; Baranova, Z.; Gauthier, S.; Reibenspies, J. H.; Gladysz, J. A. A New Type of Insulated Molecular Wire: A Rotaxane Derived from a Metal-Capped Conjugated Tetrayne. *Chem. Commun.* **2012**, *48*, 7562-7564.

(18) Bruce, M. I.; Low, P. J.: Transition Metal Complexes Containing All-Carbon Ligands. In *Advances In Organometallic Chemistry, Vol. 50*; West, R., Hill, A. F., Eds.; Advances In Organometallic Chemistry, 2004; Vol. 50; Pp 179-444.

(19) Parthey, M.; Gluyas, J. B. G.; Schauer, P. A.; Yufit, D. S.; Howard, J. A. K.; Kaupp, M.; Low, P. J. Refining The Interpretation of Near-Infrared Band Shapes in a Polyynediyl Molecular Wire. *Chemistry-A European Journal* **2013**, *19*, 9780-9784.

(20) Martin, S.; Grace, I.; Bryce, M. R.; Wang, C.; Jitchati, R.; Batsanov, A. S.; Higgins, S. J.; Lambert, C. J.; Nichols, R. J. Identifying Diversity in Nanoscale Electrical Break Junctions. *J. Am. Chem. Soc.* **2010**, *132*, 9157-9164.

(21) Leary, E.; Hobenreich, H.; Higgins, S. J.; Van Zalinge, H.; Haiss, W.; Nichols, R. J.; Finch, C. M.; Grace, I.; Lambert, C. J.; Mcgrath, R.; Smerdon, J. Single-Molecule Solvation-Shell Sensing. *Phys. Rev. Lett.* **2009**, *102*, 086801.

(22) Long, D. P.; Lazorcik, J. L.; Mantooth, B. A.; Moore, M. H.; Ratner, M. A.; Troisi, A.; Yao, Y.; Ciszek, J. W.; Tour, J. M.; Shashidhar, R. Effects of Hydration on Molecular Junction Transport. *Nat. Mater.* **2006**, *5*, 901-908.

(23) Bruce, M. I.; Nicholson, B. K.; Binshawkataly, O.; Shapley, J. R.; Henly, T. Synthesis of Gold-Containing Mixed-Metal Cluster Complexes. *Inorg. Synth.* **1989**, *26*, 324-328.

(24) Rubin, Y.; Lin, S. S.; Knobler, C. B.; Anthony, J.; Boldi, A. M.; Diederich, F. Solution-Spray Flash Vacuum Pyrolysis - A New Method for the Synthesis of Linear Poliynes with Odd Numbers Of CC Bonds From Substituted 3,4-Dialkynyl-3-Cyclobutene-1,2-Diones. *J. Am. Chem. Soc.* **1991**, *113*, 6943-6949.

(25) De Graaf, W.; Smits, A.; Boersma, J.; Van Koten, G.; Hoekstra, W. P. M. Synthesis of Marasin and 9 Methylmarasin Nona and Deca-6 8-Diyne-3 4-Dienol. *Tetrahedron* **1988**, *44*, 6699-6704.

(26) Wang, C.; Batsanov, A. S.; West, K.; Bryce, M. R. Synthesis and Crystal Structures of Isolable Terminal Aryl Hexatriyne and Octatetrayne Derivatives: Ar-(C≡C)(n)H (n=3,4). *Org. Lett.* **2008**, *10*, 3069-3072.

(27) Coulson, D. R.; Satek, L. C.; Grom, S. O. Tetrakis(Triphenylphosphine)Palladium(0), In Inorganic Syntheses, Volume 13 (Ed F. A. Cotton), John Wiley & Sons, Inc., Hoboken, NJ, USA. . **1972**, 121-124.

(28) Decicco, R. C.; Black, A.; Li, L.; Goroff, N. S. An Iterative Method for the Synthesis of Symmetric Polyynes. *Eur. J. Org. Chem.* **2012**, 4699-4704.

(29) Haiss, W.; Nichols, R. J.; Van Zalinge, H.; Higgins, S. J.; Bethell, D.; Schiffrin, D. J. Measurement of Single Molecule Conductivity Using the Spontaneous Formation of Molecular Wires. *Phys. Chem. Chem. Phys.* **2004**, *6*, 4330-4337.

(30) Haiss, W.; Van Zalinge, H.; Higgins, S. J.; Bethell, D.; Hobenreich, H.; Schiffrin, D. J.; Nichols, R. J. Redox State Dependence of Single Molecule Conductivity. *J. Am. Chem. Soc.* **2003**, *125*, 15294-15295.

(31) Nichols, R. J.; Haiss, W.; Higgins, S. J.; Leary, E.; Martin, S.; Bethell, D. The Experimental Determination of the Conductance of Single Molecules. *Phys. Chem. Chem. Phys.* **2010**, *12*, 2801-2815.

(32) Xu, B. Q.; Tao, N. J. J. Measurement of Single-Molecule Resistance by Repeated Formation of Molecular Junctions. *Science* **2003**, *301*, 1221-1223.

(33) Lambert, C. J. Basic Concepts of Quantum Interference and Electron Transport in Single-Molecule Electronics. *Chem. Soc. Rev.* **2015**, *44*, 875-888.

(34) Soler, J. M.; Artacho, E.; Gale, J. D.; Garcia, A.; Junquera, J.; Ordejon, P.; Sanchez-Portal, D. The SIESTA Method for Ab Initio Order-N Materials Simulation. *Journal Of Physics-Condensed Matter* **2002**, *14*, 2745-2779.

(35) Artacho, E.; Anglada, E.; Dieguez, O.; Gale, J. D.; Garcia, A.; Junquera, J.; Martin, R. M.; Ordejon, P.; Pruneda, J. M.; Sanchez-Portal, D.; Soler, J. M. The SIESTA Method; Developments and Applicability. *Journal Of Physics-Condensed Matter* **2008**, *20*, 064208.

(36) Ferrer, J.; Lambert, C. J.; Garcia-Suarez, V. M.; Manrique, D. Z.; Visontai, D.; Oroszlany, L.; Rodriguez-Ferradas, R.; Grace, I.; Bailey, S. W. D.; Gillemot, K.; Sadeghi, H.; Algharagholy, L. A. GOLLUM: A Next-Generation Simulation Tool for Electron, Thermal and Spin Transport. *New Journal Of Physics* **2014**, *16*, 093029.

(37) Jones, G. E.; Kendrick, D. A.; Holmes, A. B.; Armstrong, J.; Heathcock, C. H. 1,4-Bis(Trimethylsilyl)Buta-1,3-Diyne. *Org. Synth.* **1987**, *65* 52.

(38) Jones, G. E.; Kendrick, D. A.; Holmes, A. B.; Armstrong, J.; Heathcock, C. H. 1,4-Bis(Trimethylsilyl)Buta-1,3-Diyne. *Org. Synth. Coll. Vol. 8* **1993**, 63.

(39) Gao, K.; Goroff, N. S. Two New Iodine-Capped Carbon Rods. *J. Am. Chem. Soc.* **2000**, *122*, 9320-9321.

(40) Bruce, M. I.; Low, P. J.; Werth, A.; Skelton, B. W.; White, A. H. Some Transition-Metal Complexes Derived from Silylated 1,3-Diynes. *Journal Of The Chemical Society-Dalton Transactions* **1996**, 1551-1566.

(41) Antonova, A. B.; Bruce, M. I.; Elis, B. G.; Gaudio, M.; Humphrey, P. A.; Jevric, M.; Melino, G.; Nicholson, B. K.; Perkins, G. J.; Skelton, B. W.; Stapleton, B.; White, A. H.; Zaitseva, N. N. A Novel Methodology for the Synthesis of Complexes Containing Long Carbon Chains Linking Metal Centres: Molecular Structures of {Ru(Dppe)Cp*}(2)(Mu-C-14) and {Co-3(Mu-Dppm)(CO)(7)}(2)(Mu(3):Mu(3)-C-16). *Chem. Commun.* **2004**, *8*, 960-961.

(42) Antonova, A. B.; Bruce, M. I.; Humphrey, P. A.; Gaudio, M.; Nicholson, B. K.; Scoleri, N.; Skelton, B. W.; White, A. H.; Zaitseva, N. N. Alkynyl and Poly-ynyl Derivatives of Carbon-Tricobalt Clusters. *J. Organomet. Chem.* **2006**, *691*, 4694-4707.

(43) Bruce, M. I.; Bueschel, S.; Cole, M. L.; Scoleri, N.; Skelton, B. W.; White, A. H.; Zaitseva, N. N. Some Chemistry Of Trans-Ru(C≡CC≡CH)(2)(DPPE)(2): Syntheses of Bi- and Tri-Metallic Derivatives and Cycloaddition of TCNE. *Inorg. Chim. Acta* **2012**, *382*, 6-12.

(44) Man, W. Y.; Bock, S.; Zaitseva, N. N.; Bruce, M. I.; Low, P. J. Cross-Coupling Reactions of Gold(I) Alkynyl and Polyyndiyl Complexes. *J. Organomet. Chem.* **2011**, *696*, 2172-2176.

(45) Marques-Gonzalez, S.; Yufit, D. S.; Howard, J. A. K.; Martin, S.; Osorio, H. M.; Garcia-Suarez, V. M.; Nichols, R. J.; Higgins, S. J.; Cea, P.; Low, P. J. Simplifying the Conductance Profiles of Molecular Junctions: The Use of the Trimethylsilylethynyl Moiety as a Molecule-Gold Contact. *Dalton Transactions* **2013**, *42*, 338-341.

(46) Pera, G.; Martin, S.; Ballesteros, L. M.; Hope, A. J.; Low, P. J.; Nichols, R. J.; Cea, P. Metal-Molecule-Metal Junctions in Langmuir-Blodgett Films Using a New Linker: Trimethylsilane. *Chemistry-A European Journal* **2010**, *16*, 13398-13405.

(47) Wu, S. M.; Gonzalez, M. T.; Huber, R.; Grunder, S.; Mayor, M.; Schonenberger, C.; Calame, M. Molecular Junctions Based on Aromatic Coupling. *Nat. Nanotechnol.* **2008**, *3*, 569-574.

(48) Venkataraman, L.; Klare, J. E.; Tam, I. W.; Nuckolls, C.; Hybertsen, M. S.; Steigerwald, M. L. Single-Molecule Circuits with Well-Defined Molecular Conductance. *Nano Lett.* **2006**, *6*, 458-462.

(49) Li, C.; Pobelov, I.; Wandlowski, T.; Bagrets, A.; Arnold, A.; Evers, F. Charge Transport In Single Au - Alkanedithiol - Au Junctions: Coordination Geometries and Conformational Degrees of Freedom. *J. Am. Chem. Soc.* **2008**, *130*, 318-326.

(50) Xia, J. L.; Diez-Perez, I.; Tao, N. J. Electron Transport in Single Molecules Measured by a Distance-Modulation Assisted Break Junction Method. *Nano Lett.* **2008**, *8*, 1960-1964.

(51) Markopoulou, C. K.; Kouskoura, M. G.; Koundourellis, J. E. Modelling by Partial Least Squares the Relationship between the HPLC Mobile Phases and Analytes on Phenyl Column. *J. Sep. Sci.* **2011**, *34*, 1489-1502.

(52) Al-Backri, A.; Zolyomi, V.; Lambert, C. J. Electronic Properties of Linear Carbon Chains: Resolving The Controversy. *J. Chem. Phys.* **2014**, *140*, 104306.

(53) Haley, M. M. Carbon Allotropes on the Road to Carbyne. *Nature Chemistry* **2010**, *2*, 912-913.

(54) Hendon, C. H.; Tiana, D.; Murray, A. T.; Carbery, D. R.; Walsh, A. Helical Frontier Orbitals of Conjugated Linear Molecules. *Chemical Science* **2013**, *4*, 4278-4284.

(55) Manrique, D. Z.; Huang, C.; Baghernejad, M.; Zhao, X.; Al-Owaedi, O. A.; Sadeghi, H.; Kaliginedi, V.; Hong, W.; Gulcur, M.; Wandlowski, T.; Bryce, M. R.; Lambert,

C. J. A Quantum Circuit Rule for Interference Effects in Single-Molecule Electrical Junctions. *Nature Communications* **2015**, *6*.

(56) Li, X. L.; He, J.; Hihath, J.; Xu, B. Q.; Lindsay, S. M.; Tao, N. J. Conductance Of Single Alkanedithiols: Conduction Mechanism and Effect of Molecule-Electrode Contacts. *J. Am. Chem. Soc.* **2006**, *128*, 2135-2141.

(57) Li, X.; Hihath, J.; Chen, F.; Masuda, T.; Zang, L.; Tao, N. Thermally Activated Electron Transport in Single Redox Molecules. *J. Am. Chem. Soc.* **2007**, *129*, 11535-11542.

(58) Cao, H.; Jiang, J.; Ma, J.; Luo, Y. Temperature-Dependent Statistical Behavior of Single Molecular Conductance in Aqueous Solution. *J. Am. Chem. Soc.* **2008**, *130*, 6674-6675.

(59) Fatemi, V.; Kamenetska, M.; Neaton, J. B.; Venkataraman, L. Environmental Control of Single-Molecule Junction Transport. *Nano Lett.* **2011**, *11*, 1988-1992.

TABLE OF CONTENTS GRAPHIC